# Efficient transient stability analysis of electrical power system based on a spatially paralleled hybrid approach

**Abstract—With continually increasing complexities of power systems, transient stability analysis as an important task for system security operation becomes very time-consuming and thus an efficient analysis tool is urgently needed. In this paper, a spatially paralleled hybrid approach combining the high-order Taylor series algorithm and the block bordered diagonal form (BBDF) was proposed to improve the computational efficiency of power system transient stability analysis. The proposed approach only exchanged high-order derivatives of generator voltages and currents between partitioned power network subsystems and the coordinated-bus cluster based on BBDF, and enhanced the triangular factorization recursive utilization rate of admittance matrix using the Taylor series algorithm with a large integration step. Finally, the proposed spatially paralleled hybrid approach was tested in the New England 39-bus, IEEE 145-bus and an expanded 580-bus systems, and simulation results have validated the proposed approach is very effective and computationally efficient for power system transient stability analysis.**

***Index Terms*— Transient stability analysis; high-order Taylor series algorithm; block bordered diagonal form; spatially paralleled hybrid approach**

## I. INTRODUCTION

Power system transient stability is always an important issue for power system security operation especially in an environment of stressed power system networks [1, 2]. With continually rising complexities and increasing scales of electrical power systems, transient stability analysis becomes more time-consuming than ever before [3, 4], and an efficient transient stability analysis method is in a pressing need for power system on-line security analysis and preventive control.

As transient stability analysis is essentially to solve a large set of high-dimensional nonlinear Differential Algebraic Equations (DAEs) by using an integration algorithm, the time cost for conducting these simulations is usually very high. In order to ameliorate the transient stability analysis, one strategy is to develop competent mathematical integration algorithms such as the implicit trapezoid method, the Euler method [5, 6] , Gear method [7, 8] and the high-order Taylor series method [9, 10] etc. for solving DAEs. In [5], the paper utilized the Euler integration based 'Dynamic Computation for Power Systems' software package to analyze the effect of fault locations and critical clearing time on the transient stability of the IEEE 14-bus system, while [9] adopted the high-order derivative method for on-line transient stability evaluation for the classical non-salient pole generator with constant network admittance matrices. Reference [10] further enhanced the efficiency of high-order Taylor series algorithm by dynamic controlling the derivative order of state variables. Based on Taylor expansion, multiple group equivalences for generators were proposed in [11] to reduce the number of DAEs and thus alleviate the computational burden. On the other hand, with the development of computer technology, developing paralleled or distributed computation strategy is another option to boost the efficiency of transient stability analysis. Recently much attention has been paid to exploring modern advanced computing techniques for on-line paralleled or distributed transient stability analysis [12, 13].

There are three typical paralleled or distributed transient stability analysis strategies, i.e., the spatial [14-19] parallelization, the temporal parallelization [20-22] and the hybrid spatiotemporal parallelization [23, 24]. 1) For spatial parallelization, authors [14] partitioned the original system into several subsystems by the geographical decomposition technique and Conjugate Gradient methods respectively, and then utilized the lower-triangular and upper-triangular factorization to form a spatially paralleled transient stability analysis method. In [15] a new architecture layout based on distributed IBM clusters was proposed for a real-time power system simulation. In [17], an eigenvector-based partitioning technique was designed to enhance the performance of waveform relaxation method for fast analysis of complex power systems transient stability. Authors of [16, 18, 19] proposed a novel multi-level partition scheme for parallel computing and designed a block bordered diagonal form (BBDF) based hierarchical algorithm for transient stability computation. Due to more balanced and reasonable partition scheme for subsystems, the computation and communication time was effectively reduced. 2) For temporal parallelization, a distributed computing approach for temporal parallel transient stability analysis was presented in [21] with two parts: the functional decomposition obtained by the Shifted-Picard algorithm and the domain decomposition obtained by concurrent running multiple contingencies on computer clusters. Prof. Wang also adopted the Shifted-Picard dynamic iterations in [22] to conduct a parallel transient stability analysis, and solved the DAEs by integrating several integration steps simultaneously instead of just integrating a single step. 3) For hybrid spatiotemporal parallelization, authors in [23] designed a new parallel transient stability analysis algorithm with the help of the relaxed Newton strategy, and reached a compromise between the convergence speed and the parallelization efficiency. In [24] a Jacobi-free Newton-GMRES algorithm by using heterogeneous computing resources was proposed for the distributed transient stability analysis of interconnected power systems. Indeed, all these three typical parallel strategies greatly speed up the transient stability analysis. However, as they merely solved the DAEs using low order derivative-based integration

such as the Euler or trapezoidal method, there is still large gaps for further improving the analysis efficiency and accuracy by incorporating the high-order derivative integration method with parallel computation techniques.

Therefore, with advantages of the parallel computation and high-order Taylor series algorithm of large integration steps for DAEs, this paper proposed a spatially paralleled hybrid approach incorporating the high-order Taylor series with the block bordered diagonal form (BBDF) to improve power system transient stability analysis. The main contributions of this paper include: 1) an original spatially paralleled hybrid approach simultaneously taking advantages of the high-order Taylor series algorithm and the BBDF is presented for power system transient stability analysis with a salient-pole generator model considered; 2) the proposed approach only needs to exchange limited key boundary high-order derivatives of generator variables between power sub-networks and the coordinated-bus cluster based on BBDF and thus it is with a good data privacy; 3) the proposed method can also enhance the triangular factorization reuse efficiency with a large integration step and thus it is very efficient for transient stability analysis; 4) the proposed approach is very flexible to incorporate any dynamic components for power system transient stability analysis; 5) based on the platform which is conveniently configured with computer clusters and Matlab Distributed Computing Server, three general case studies are conducted to validate the accuracy and efficiency of the proposed approach for transient stability analysis.

The paper is organized as follows. The BBDF is briefly introduced in Section II. The proposed spatially paralleled hybrid approach with a detailed calculation procedure is presented in Section III. Three case studies are investigated in Section IV with a conclusion drawn in the last section.

## II. BLOCK BORDERED DIAGONAL FORM

The DAEs for power system transient stability analysis could be generally described as [25]

$$\begin{cases} X' = F(\mathbf{X},\mathbf{Z},t) \\ 0 = G(\mathbf{X},\mathbf{Z},t) \end{cases} \tag{1}$$

where $\mathbf{X}$ and $\mathbf{Z}$ stand for the state variables and algebraic variables respectively. The state variables $\mathbf{X}$ in DAEs (1) are independent of each other in the viewpoint of differential equations $F(\mathbf{X},\mathbf{Z},t)$, and they are merely coupled by algebraic variables $\mathbf{Z}$ in $G(\mathbf{X},\mathbf{Z},t)$. Therefore, the crux of parallel transient stability analysis is to solve the network equations for algebraic variables $\mathbf{Z}$ in parallel. In power systems, the network equations $G(\mathbf{X},\mathbf{Z},t)$ are used to describe the relationships between nodal voltages and currents as (2)

$$\mathbf{YV} = \mathbf{I} \tag{2}$$

where $\mathbf{Y}$ stands for power network admittance matrix, $\mathbf{V}$ and $\mathbf{I}$ are nodal voltages and injected currents, respectively. Since the admittance matrix of practical power systems is a highly sparse one, equation (2) could always be reordered through proper row and column permutations resulting in the block bordered diagonal form (BBDF) as (3), which has been used in many fields of parallel calculation such as for power flow calculation [26] and power system transient stability simulation [16, 27].

$$\begin{pmatrix} \mathbf{Y}_{11} & \mathbf{0} & \cdots & \mathbf{0} & \mathbf{Y}_{1t} \\ \mathbf{0} & \mathbf{Y}_{22} & \cdots & \mathbf{0} & \mathbf{Y}_{2t} \\ \vdots & \vdots & \ddots & \vdots & \vdots \\ \mathbf{0} & \mathbf{0} & \cdots & \mathbf{Y}_{kk} & \mathbf{Y}_{kt} \\ \mathbf{Y}_{t1} & \mathbf{Y}_{t2} & \cdots & \mathbf{Y}_{tk} & \mathbf{Y}_{tt} \end{pmatrix} \begin{pmatrix} \mathbf{V}_1 \\ \mathbf{V}_2 \\ \vdots \\ \mathbf{V}_k \\ \mathbf{V}_t \end{pmatrix} = \begin{pmatrix} \mathbf{I}_1 \\ \mathbf{I}_2 \\ \vdots \\ \mathbf{I}_k \\ \mathbf{I}_t \end{pmatrix} \tag{3}$$

In (3),$\mathbf{V}_j$ ($j$=1,2,…,$k$) and $\mathbf{I}_j$ ($j$=1,2,…,$k$) are the nodal voltage and current of subsystem $j$; $\mathbf{Y}_{jj}$ ($j$=1,2,…,k) is the admittance matrix of subsystem $j$. $\mathbf{V}_t$ and $\mathbf{I}_t$ are the splitting voltage and current variables between the subsystems and the coordinated-bus cluster; $\mathbf{Y}_{tt}$ is the admittance matrix of coordinated cluster. From (3), it is clear that variables in each subsystem are only coupled with the split voltage $\mathbf{V}_t$. If $\mathbf{V}_t$ is known, the voltage of other subsystems could be easily calculated in parallel. Based on (3), the equations for coordinated cluster can be solved by (4)

$$\mathbf{Y}_{tt}'\mathbf{V}_t = \mathbf{I}_t' \tag{4}$$

where $\mathbf{Y}_{tt}' = \mathbf{Y}_{tt} - \sum_{j=1}^{k} \mathbf{Y}_{tj}\mathbf{Y}_{jj}^{-1}\mathbf{Y}_{jt}$, $\mathbf{I}_t' = \mathbf{I}_t - \sum_{j=1}^{k} \mathbf{Y}_{tj}\mathbf{Y}_{jj}^{-1}\mathbf{I}_j$.

If the splitting voltage $\mathbf{V}_t$ in (4) has been obtained, the voltage $\mathbf{V}_j$ of each subsystem in (3) could be sutured as

$$\mathbf{V}_j = \mathbf{Y}_{jj}^{-1}(\mathbf{I}_j - \mathbf{Y}_{jt}\mathbf{V}_t) \ (j = 1,2,\cdots,k) \tag{5}$$

From the above analysis, the BBDF strategy for parallel calculating the algebraic variables $\mathbf{Z}$ of power network equations $G(\mathbf{X},\mathbf{Z},t)$ mainly includes two steps: 1) each subsystem sends out the equivalent variables $\mathbf{Y}_{tj}$, $\mathbf{Y}_{jj}^{-1}$, $\mathbf{Y}_{jt}$ and $\mathrm{I}_j$ to the coordinated cluster, then the splitting voltage $\mathbf{V}_t$ could be readily calculated by (4); 2) the coordinated cluster sends back the splitting voltage $\mathbf{V}_t$ to each subsystem, and the voltage $\mathbf{V}_j$ ($j$=1,2,…,$k$) in each subsystem is computed in parallel by (5). Based on BBDF, a large-scale power network equation $G(\mathbf{X},\mathbf{Z},t)$ for complex power systems could be portioned into multiple subsections and solved in parallel, thus BBDF could enhance the efficiency of solving network equations in a divide and conquer manner.

## III. PROPOSED SPATIALLY PARALLELED HYBRID APPROACH BASED ON TAYLOR SERIES ALGORITHM AND BBDF

Currently, the typical parallel mathematical methods for transient stability analysis are usually based on low order derivatives, such as by using Euler or trapezoidal integration method with small integration step. On the other hand, many researches indicated the high-order Taylor series algorithm could adopt a very large integration step to solve differential equations. However, in the state-of-art this high-order Taylor series method has not taken the advantage of parallel computation techniques. Therefore in this section a spatially paralleled hybrid approach harvesting the merits of high-order Taylor series and the parallel computation is designed to enhance the transient stability computational efficiency. In the following, the high-order Taylor series method is firstly presented with the hybrid approach proposed afterwards.

### *A) Dynamic model for transient stability analysis*

A general salient-pole dual-axis generator model is adopted for transient stability analysis in this paper, while load demand is model as constant impedance. Rotor dynamics

of a generator are usually described by the differential equations (6) for power system transient stability.

$$\frac{d\delta_i}{dt} = \omega_i \tag{6a}$$

$$M_i \frac{d\omega_i}{dt} = P_{mi} - P_{ei} - D\omega_i \tag{6b}$$

$$T_{di}^{'} \frac{dE_{qi}^{'}}{dt} = -E_{qi}^{'} + (X_{di}^{'} - X_{di})I_{di} + E_{fdi} \tag{6c}$$

$$T_{qi}^{'} \frac{dE_{di}^{'}}{dt} = -E_{di}^{'} + (X_{qi} - X_{qi}^{'})I_{qi} \tag{6d}$$

where $M$ is the generator inertial constant; $\delta_i$ and $\omega_i$ are $i^{\text{th}}$ generator angles and speeds in per unit; $P_{mi}$ and $P_{ei}$ are generator mechanical and electromagnetic power respectively; $D$ is the damping ratio; $I_{di}$ and $I_{qi}$ are the $d$ and $q$ stator currents; $T_{di}^{'}$ and $T_{qi}^{'}$ are the $d$ and $q$ transient time constant; $X_{di}^{'}$, $X_{qi}^{'}$, $X_{di}$ and $X_{qi}$ are the $d$ and $q$ transient and synchronous reactance; $E_{di}^{'}$ and $E_{qi}^{'}$ are the $d$ and $q$ transient potential voltage.

The dynamic admittance matrix $\hat{\mathbf{Y}}_g(\boldsymbol{\delta})$ related to generator angle $\delta$ is a diagonal matrix defined as

$$\hat{\mathbf{Y}}_g(\boldsymbol{\delta}) = diag\left(Y_g(\delta_1) \quad Y_g(\delta_2) \quad \cdots \quad Y_g(\delta_n)\right) \tag{7}$$

and

$$Y_g(\delta_i) = \frac{1}{R_{ai}^2 + X_{qi}^{'}X_{di}^{'}} \begin{pmatrix} R_{ai} - (X_{di}^{'} - X_{qi}^{'})\sin 2\delta_i/2 & (X_{di}^{'} + X_{qi}^{'})/2 + (X_{di}^{'} - X_{qi}^{'})\cos 2\delta_i/2 \\ -(X_{di}^{'} + X_{qi}^{'})/2 + (X_{di}^{'} - X_{qi}^{'})\cos 2\delta_i/2 & R_{ai} + (X_{di}^{'} - X_{qi}^{'})\sin 2\delta_i/2 \end{pmatrix} \tag{8}$$

where $R_{ai}$, $X_{di}^{'}$ and $X_{qi}^{'}$ are the generator stator resistance, $d$ and $q$ transient reactance, respectively.

The generator Norton equivalent current vector $\hat{\mathbf{J}}_n$ could be described by (9)

$$\hat{\mathbf{J}}_n = \left(\hat{J}_1^n \quad \hat{J}_2^n \quad \cdots \quad \hat{J}_n^n\right)^{\mathrm{T}} \tag{9}$$

$$\hat{J}_i^n = \begin{pmatrix} J_{xi} \\ J_{yi} \end{pmatrix} = T(\delta_i) \frac{1}{R_{ai}^2 + X_{di}^{'}X_{qi}^{'}} \begin{pmatrix} R_{ai} & -X_{di}^{'} \\ X_{qi}^{'} & R_{ai} \end{pmatrix} \begin{pmatrix} E_{qi}^{'} \\ E_{di}^{'} \end{pmatrix} \tag{10}$$

In (10), $T(\delta_i) = \begin{pmatrix} \cos\delta_i & \sin\delta_i \\ \sin\delta_i & -\cos\delta_i \end{pmatrix}$ is the axis transfer matrix between $x$-$y$ and $d$-$q$ axis, and $(E_{qi}^{'}, E_{di}^{'})^T$ are the generator $q$ and $d$ axis transient voltage behind the transient reactance, respectively.

Based on (7) and (9), the power network equations coupled with the dual-axis generator [25] are

$$\left(\hat{\mathbf{Y}}_n + \hat{\mathbf{Y}}_g(\boldsymbol{\delta})\right)\hat{\mathbf{V}}_n = \hat{\mathbf{J}}_n \quad \text{or} \quad \mathbf{I}_n = \hat{\mathbf{Y}}_n\hat{\mathbf{V}}_n = \hat{\mathbf{J}}_n - \hat{\mathbf{Y}}_g(\boldsymbol{\delta}) * \hat{\mathbf{V}}_n \tag{11}$$

where $\hat{\mathbf{Y}}_n$ is the constant admittance matrix excluding the part related to generator angle $\delta$, and its element is $\hat{\mathbf{Y}}_{ij} = \begin{pmatrix} G_{ij} & -B_{ij} \\ B_{ij} & G_{ij} \end{pmatrix}$; $\hat{\mathbf{V}}_n$ and $\mathbf{I}_n$ are the generator terminal voltage and current vector with the $i^{\text{th}}$ element as $(V_{xi}, V_{yi})^T$ and $(I_{xi}, I_{yi})^T$ ($i$=1,2,…,$n$). Formula (11) could also be rewritten as (12) for generator $i$

$$\begin{pmatrix} I_{xi} \\ I_{yi} \end{pmatrix} = \begin{pmatrix} J_{xi} \\ J_{yi} \end{pmatrix} - Y_g(\delta_i) \begin{pmatrix} V_{xi} \\ V_{yi} \end{pmatrix} \tag{12}$$

It is clear that the generator terminal current can be calculated based on the generator Norton equivalent current and terminal voltage $(V_{xi}, V_{yi})^T$, afterwards the electromagnetic power of generator $i$ could be readily calculated by $P_{ei} = V_{xi}I_{xi} + V_{yi}I_{yi}$.

***B) Calculation for high-order derivatives of generator variables***

When using high order Taylor series algorithm for transient stability analysis, the high-order derivatives of generator angles are required, and they could be derived by taking derivative of (6b) on both sides

$$\begin{aligned} \delta_i^{(1)} &= \omega_i \\ \delta_i^{(2)} &= \frac{1}{M_i}\left(P_{mi} - P_{ei} - D_i\delta_i^{(1)}\right) \\ \delta_i^{(m)} &= -\frac{1}{M_i}\left(P_{ei}^{(m-2)} + D_i\delta_i^{(m-1)}\right) \quad (m \geq 3) \end{aligned} \tag{13}$$

For transient stability analysis, the simulation time period is usually 2-5s and the mechanical power could be assumed constant, thus high-order derivatives of generator angle only depends on the high-order derivatives of electromagnetic power as shown in the third equation of (13).

Taylor series algorithm could be used to establish the recursive relationship of generator angles at time $t_{k+1}$ and the high-order derivatives of generator angle at $t_k$ for transient stability analysis. Based on the high-order derivatives of generator angles (13), generator angles at $t_{k+1}$ are calculated as

$$\delta_i(t_{k+1}) = \sum_{j=0}^{m} \delta_i^{(j)}(t_k)\frac{h^j}{j!} + O(h^{m+1}) \tag{14}$$

where $h$ is the integration step $h$=$t_{k+1}$-$t_k$ and $\boldsymbol{O}(h^{m+1})$ is the high-order infinitesimal term of Taylor series. It is noted that, the Taylor series algorithm degenerates to the Euler method as $\delta_i(t_{k+1}) = \delta_i(t_k) + \delta_i^{(1)}(t_k) * h + O(h^2)$ when $m$=1 in (14).

The numerical stability of one integration method is very important for its practical utilization of correctly solving ordinary differential equations, which concerns whether the round-off errors and/or small fluctuations in initial data cause a large deviation of final answer from the exact solution. For an ordinary differential equation $dy/dt = \lambda y$ $(\lambda < 0)$, the numerical stability region of Taylor series (14) is constrained by the following inequality [28, 29].

$$\left|1 + \lambda h + \frac{(\lambda h)^2}{2!} + \ldots + \frac{(\lambda h)^m}{m!}\right| < 1 \tag{15}$$

and the maximal integration step ensuring the numerical stability could be numerically calculated from the above inequality formula. From (15), it is clear that with the increasing derivative order $m$, the stable integration step is increased as well. As a specific case, for Euler method with $m$=1, (15) degenerates to $|1 + \lambda h| < 1$, the maximal stable integration step is correspondingly obtained as $h < 2/|\lambda|$.

To calculate the high-order derivatives of $P_{ei}$ in (13), successively differentiate both sides of electromagnetic power $P_{ei} = V_{xi}I_{xi} + V_{yi}I_{yi}$, then

$$P_{ei}^{(m)} = \sum_{k=0}^{m} C_m^k (V_{xi}^k I_{xi}^{(m-k)} + V_{yi}^k I_{yi}^{(m-k)}) \tag{16}$$

where $C_m^k = m!/[k!(m-k)!]$ is the combinatorial number. It is clear that the high-order derivatives of electromagnetic power in (16) are dependent on the high-order derivatives of generator terminal voltages and currents, which will be discussed in detail as follows.

**1）Derivatives of generator terminal voltage**

Taking derivatives of both sides of (11) and adopting binomial theorem, the high-order derivatives of Norton current can be calculated as

$$\begin{aligned} \hat{\mathbf{J}}_n^{(m)} &= \left[\left(\hat{\mathbf{Y}}_n + \hat{\mathbf{Y}}_g(\boldsymbol{\delta})\right)\hat{\mathbf{V}}_n\right]^{(m)} = \sum_{k=0}^{m} C_m^k [\hat{\mathbf{Y}}_n + \hat{\mathbf{Y}}_g(\boldsymbol{\delta})]^{(m-k)} \hat{\mathbf{V}}_n^{(k)} \\ &= \left(\hat{\mathbf{Y}}_n + \hat{\mathbf{Y}}_g(\delta)\right)\hat{\mathbf{V}}_n^{(m)} + \sum_{k=0}^{m-1} C_m^k \left(\hat{\mathbf{Y}}_n + \hat{\mathbf{Y}}_g(\delta)\right)^{(m-k)} (\delta)\hat{\mathbf{V}}_n^{(k)} \end{aligned} \tag{17}$$

Note the high-order derivative of the constant admittance is $\hat{\mathbf{Y}}_n^{(m)} = 0$, thus (17) could be simplified as

$$\left(\hat{\mathbf{Y}}_n + \hat{\mathbf{Y}}_g(\delta)\right)\hat{\mathbf{V}}_n^{(m)} = \hat{\mathbf{J}}_n^{(m)} - \sum_{k=0}^{m-1} C_m^k \hat{\mathbf{Y}}_g^{(m-k)}(\delta)\hat{\mathbf{V}}_n^{(k)} = \hat{\mathbf{J}}_n'^{(m)} \tag{18}$$

From (18), it is clear that the $m^{\text{th}}$ order derivative of generator terminal voltage $\hat{\mathbf{V}}_n^{(m)}$ depends on the generator terminal voltage derivatives $\hat{\mathbf{V}}_n^{(k)}$ for $k$=0,1,2,…,$m$-1, the $m^{\text{th}}$ order derivatives of Norton equivalent current $\hat{\mathbf{J}}_n^{(m)}$ and the high-order derivatives of generator dynamic admittance $\hat{\mathbf{Y}}_g^{(m-k)}(\delta)$ ($k$=0,1,2,…,$m$-1), while the latter two could be calculated by the following three steps.

***Step (1)**: derivatives of axis transfer matrix*

To calculate generator dynamic admittance $Y_g^{(m)}(\delta_i)$, the high-order derivatives of the axis transfer matrix $T(\delta_i) = \begin{pmatrix} \cos\delta_i & \sin\delta_i \\ \sin\delta_i & -\cos\delta_i \end{pmatrix}$ needs to be computed, and its first order derivative is

$$T^{(1)}(\delta_i) = \delta_i^{(1)} \begin{pmatrix} 0 & -1 \\ 1 & 0 \end{pmatrix} \begin{pmatrix} \cos\delta_i & \sin\delta_i \\ \sin\delta_i & -\cos\delta_i \end{pmatrix} = \begin{pmatrix} 0 & -1 \\ 1 & 0 \end{pmatrix} \delta_i^{(1)} T(\delta_i) \tag{19}$$

Taking derivatives on both sides of (19), the high-order derivatives of the axis transfer matrix are

$$T^{(m)}(\delta_i) = \begin{pmatrix} 0 & -1 \\ 1 & 0 \end{pmatrix} \sum_{k=0}^{m-1} C_{m-1}^k T^{(k)}(\delta_i) \delta_i^{(m-k)} \tag{20}$$

where $C_{m-1}^k = (m-1)!/[k!(m-k-1)!]$ is the combinatorial number.

***Step (2)**: derivatives of generator dynamic admittance*

From the definition of the generator dynamic admittance (8), the first order derivative of dynamic admittance $Y_g(\delta_i)$ is

$$\begin{aligned} Y_g^{(1)}(\delta_i) &= \frac{(X_{qi}' - X_{di}')}{R_{ai}^2 + X_{qi}' X_{di}'} \begin{pmatrix} \cos 2\delta_i & \sin 2\delta_i \\ \sin 2\delta_i & -\cos 2\delta_i \end{pmatrix} \delta_i^{(1)} \\ &= \frac{(X_{qi}' - X_{di}')}{R_{ai}^2 + X_{qi}' X_{di}'} \begin{pmatrix} 0 & 0.5 \\ -0.5 & 0 \end{pmatrix} T^{(1)}(2\delta_i) \end{aligned} \tag{21}$$

and the high-order derivatives of $Y_g(\delta_i)$ could be similarly calculated as (22) by taking derivatives on both sides of (21).

$$Y_g^{(m)}(\delta_i) = \frac{(X_{qi}' - X_{di}')}{R_{ai}^2 + X_{qi}' X_{di}'} \begin{pmatrix} 0 & 0.5 \\ -0.5 & 0 \end{pmatrix} T^{(m)}(2\delta_i) \tag{22}$$

***Step (3)**: derivatives of Norton equivalent currents*

From (10), the derivatives of generator Norton equivalent current in *x*-*y* axis could be calculated as (23) by successively differentiating both sides of (10)

$$\left(\hat{J}_i^n\right)^{(m)} = \begin{pmatrix} J_{xi} \\ J_{yi} \end{pmatrix}^{(m)} = \frac{1}{R_{ai}^2 + X_{di}' X_{qi}'} \sum_{k=0}^{m} C_m^k T^{(m-k)}(\delta_i) \begin{pmatrix} R_{ai} & -X_{di}' \\ X_{qi}' & R_{ai} \end{pmatrix} \begin{pmatrix} E_{qi}' \\ E_{di}' \end{pmatrix}^{(k)} \tag{23}$$

In (23), the calculation of high-order derivatives of $(E_{qi}', E_{di}')^T$ depends on the specific excitation system model connected at the generator for $E_{fdi}$ in 6(c) and 6(d). For example, when a generator is equipped with the IEEE type I excitation system as shown in Appendix, its high-order derivatives could be calculated by (A1) to (A5). For other typical excitation systems, the high-order derivatives of dynamic potential voltage $(E_{qi}', E_{di}')^T$ could be similarly derived from the differential equations of excitation system.

With **step *(1), (2)* and *(3)***, the high-order derivatives of generator terminal voltage could be calculated by (18).

**2) Derivatives of generator terminal current**

The high-order derivatives of the $i^{\text{th}}$ generator's terminal current $I_i = (I_{xi}, I_{yi})^{\text{T}}$ could be calculated as (24) by taking derivatives of (12) on both sides

$$\begin{pmatrix} I_{xi} \\ I_{yi} \end{pmatrix}^{(m)} = \begin{pmatrix} J_{xi} \\ J_{yi} \end{pmatrix}^{(m)} - \sum_{k=0}^{m} C_m^k Y_g^{(m-k)}(\delta_i) \begin{pmatrix} V_{xi} \\ V_{yi} \end{pmatrix}^{(k)} \tag{24}$$

where the high-order derivatives of generator Norton equivalent current $((J_{xi}, J_{yi})^{(m)})^T$ has already been calculated by (23), and the high-order voltage derivatives $((V_{xi}, V_{yi})^{(k)})^{\text{T}}$ ($k$=0,1,…,$m$) has already been solved by (18).

**3) Derivatives of generator electromagnetic power**

With the current and the voltage derivatives addressed by (24) and (18), the high-order derivatives of electromagnetic power in (16) could be easily computed.

***C) Spatially paralleled hybrid approach***

From the above analysis, the high-order derivatives of generator state variables could be calculated separately for each generator from equations (13)-(14) and (19)-(24) (as $i^{\text{th}}$ generator is only dependent on the variables with the subscript $i$), if the equations (18) representing the coupling of physical power networks are solved. Therefore, in order to form a high-order Taylor series based parallel approach for transient stability analysis, the key is to decouple the power network equation and solve the high-order derivatives of generator terminal voltage from (18) in parallel. With BBDF introduced in Section II, the equation (18) could be rearranged as (25).

$$\begin{pmatrix} \hat{\mathbf{Y}}_{11} & \mathbf{0} & \cdots & \mathbf{0} & \hat{\mathbf{Y}}_{1t} \\ \mathbf{0} & \hat{\mathbf{Y}}_{22} & \cdots & \mathbf{0} & \hat{\mathbf{Y}}_{2t} \\ \vdots & \vdots & \ddots & \vdots & \vdots \\ \mathbf{0} & \mathbf{0} & \cdots & \hat{\mathbf{Y}}_{kk} & \hat{\mathbf{Y}}_{kt} \\ \hat{\mathbf{Y}}_{t1} & \hat{\mathbf{Y}}_{t2} & \cdots & \hat{\mathbf{Y}}_{tk} & \hat{\mathbf{Y}}_{tt} \end{pmatrix} \begin{pmatrix} \hat{\mathbf{V}}_1 \\ \hat{\mathbf{V}}_2 \\ \vdots \\ \hat{\mathbf{V}}_k \\ \hat{\mathbf{V}}_t \end{pmatrix}^{(m)} = \begin{pmatrix} \hat{\mathbf{J}}_1' \\ \hat{\mathbf{J}}_2' \\ \vdots \\ \hat{\mathbf{J}}_k' \\ \hat{\mathbf{J}}_t' \end{pmatrix}^{(m)} \tag{25}$$

and it could be calculated in parallel as (26) and (27).

$$\begin{aligned} \mathbf{Y}_{tt}' \hat{\mathbf{V}}_t^{(m)} &= \mathbf{I}_t'^{(m)} \\ \mathbf{I}_t'^{(m)} &= \hat{\mathbf{J}}_t'^{(m)} - \sum_{j=1}^{k} \mathbf{Y}_{tj} \mathbf{Y}_{jj}^{-1} \hat{\mathbf{J}}_j'^{(m)} \\ \mathbf{Y}_{tt}' &= \mathbf{Y}_{tt} - \sum_{j=1}^{k} \mathbf{Y}_{tj} \mathbf{Y}_{jj}^{-1} \mathbf{Y}_{jt} \end{aligned} \tag{26}$$

and

$$\hat{\mathbf{V}}_j^{(m)} = \mathbf{Y}_{jj}^{-1} (\mathbf{J}_j'^{(m)} - \mathbf{Y}_{jt} \hat{\mathbf{V}}_t^{(m)}) \quad (j=1,2,\ldots,k) \tag{27}$$

where 1-$k$ is the index of subsystem, $t$ is the index of coordinated-bus cluster, $\hat{\mathbf{J}}'_j$ ($j$=1,2,…,$k$) and $\hat{\mathbf{J}}'_t$ are the sub-vectors of $\hat{\mathbf{J}}'_n$ in (18), $\hat{\mathbf{Y}}_{jj}$, $\hat{\mathbf{Y}}_{jt}$, $\hat{\mathbf{Y}}_{tj}$ and $\hat{\mathbf{Y}}_{tt}$ are sub-matrices of the admittance matrix $\left(\hat{\mathbf{Y}}_n+\hat{\mathbf{Y}}_g(\delta)\right)$. With BBDF, each subsystem firstly submits the equivalent derivatives $\hat{\mathbf{J}}'^{(m)}_j$ and the admittance matrix $\hat{\mathbf{Y}}_{tj}$, $\mathbf{Y}^{-1}_{jj}$ to the coordinated cluster for solving the high-order derivatives of splitting voltage $\hat{\mathbf{V}}^{(m)}_t$ by (26); afterwards the coordinated cluster sends back $\hat{\mathbf{V}}^{(m)}_t$ to each subsystem, then the subsystem calculates the high-order voltage derivatives $\hat{\mathbf{V}}^{(m)}_j$ ($j$=1,2,…,$k$) by (27) in parallel. In practice, in order to balance the complexity and computational burden among different subsystems for solving (27), the original power network should be decomposed into several subsystems with roughly equal block sizes and small borders. For this purpose, the graph partitioning tool METIS [30] was used to produce high quality partitions in this paper.

To sum up, the flowchart for the proposed spatially paralleled hybrid approach for transient stability analysis is provided in Fig. 1, in which the blue and red dashed boxes highlight the steps for calculating the high-order derivatives and solving the power network in parallel respectively.

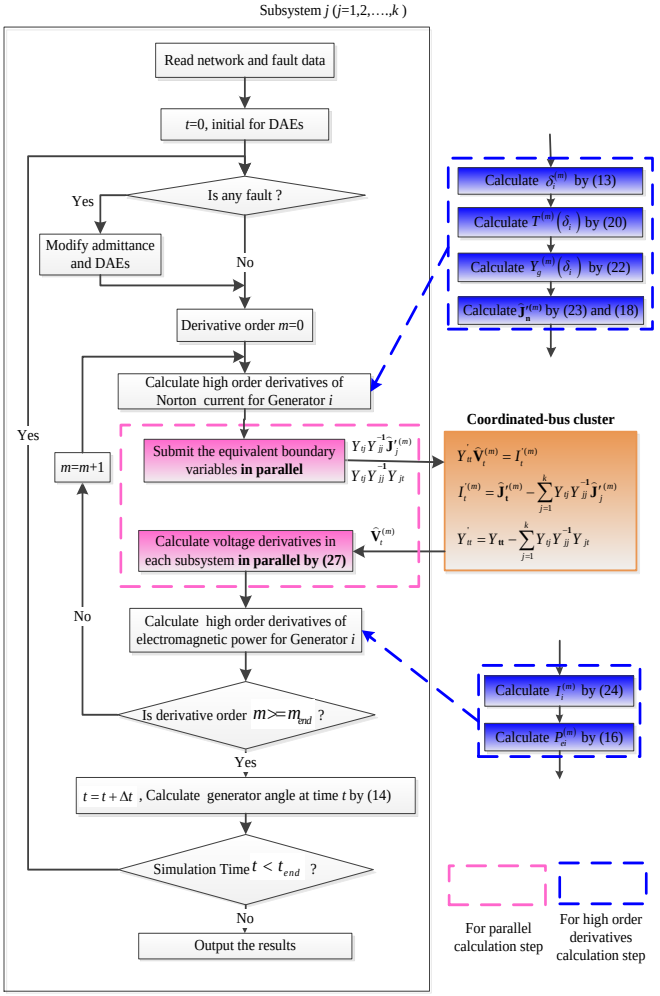


Fig. 1 Flowchart of proposed hybrid approach

### *D) Strategy for the trade-off between the integration step and derivative order*

The computational burden of proposed Taylor series algorithm for transient stability analysis is closely dependent on the integration step size and the derivative order. In the following, a general computational burden index will be introduced to determine the trade-off between the integration step and derivative order of Taylor method for transient stability analysis.

Based on the investigations in [10], the computational burden of one procedure could be approximately quantified by the numbers of multiplication calculations. To conduct the transient stability analysis of a power network with $N_g$ generators under a single contingency, the computational cost merely at one integration step of time domain simulation can be divided into three parts:

1) the burden of computing the triangular factorization matrix is

$$C_1=\frac{1}{3}\times[8\times(N_g+1)^3+4\times(N_g+1)] \tag{28}$$

2) the burden of solving network equations by forward and backward iterations is

$$C_2=4\times(N_g+1)^2-1 \tag{29}$$

3) the burden to obtain the $m^{th}$ order derivatives for $N_g$ generators is

$$C_3=(38m+27)\times N_g \tag{30}$$

With (28)-(30), the computational cost of using the $p$-order Taylor method at one single integration step includes: 1) conducting the triangular factorization for one time; 2) solving network equations for $p$+1 times; 3) and obtaining the high order derivatives for $p$+1 times, and therefore the computational cost at one step could be estimated by (31)

$$\begin{aligned} C_{Taylor}&=C_1+\sum_{m=0}^{p}(C_2+C_3)=19N_g p^2+[4(N_g+1)^2+46N_g-1]p \\ &+4(N_g+1)^2+27N_g-1+\frac{[8\times(N_g+1)^3+4\times(N_g+1)]}{3} \end{aligned} \tag{31}$$

When adopting an integration algorithm to solve DAEs for transient stability analysis, the integration step is nonlinearly constrained by the numerical stability region of the algorithm and is also strongly nonlinear to the required accuracy of DAEs' state variables solved for transient stability analysis. Due to the complicated dynamics in time domain simulation, it is intractable to seek out an explicit expression of the integration step to satisfy the required accuracy. With regard to the $p$-order Taylor method for transient stability analysis in this paper, which is specially contained by the numerical stability region (15) and prefixed accuracy of generator angles, the appropriate integration step is determined by a dichotomy strategy and denoted as $h_p$ here. Based on these discussions, the total calculation cost of $p$-order Taylor method for transient stability in timespan $T$ is calculated as the total numbers of integration steps multiplying the computational burden in one single integration step, namely by (32)

$$C_{total}=T/h_p * C_{Taylor} \tag{32}$$

Based on (32), the derivative order with the minimum computational burden $C_{total}$ would be the optimal order for the transient stability analysis during timespan $T$, and therefore formula (32) could be used as an approximate strategy to

search the trade-off between the integration step and derivative orders. This strategy of (32) would be investigated and discussed in details for three case studies in Section IV.

It is also noted that there is not a general correlation between the network scale and optimal derivative orders such as a bigger network associated with higher optimal derivative orders. According to (32), the computational cost is closely related to the appropriate integration step $h_p$, which is nonlinearly determined by the numerical stability region of an integration algorithm and the required accuracy of time domain simulation. For power networks with different time-scale power generator dynamic models and control systems, $h_p$ is very different for the same accuracy requirements, and the optimal derivative order can only be figured out at the trade-off point with the minimum calculation burden according to (32). This statement would be further elaborated by the optimal derivative orders of IEEE 145-bus, 580-bus, 870-bus and 1160-bus system in the next section.

As the byproducts of the computational burden analysis for proposed approach, the computational cost of the Runge-Kutta method and Newton-Raphson embedded trapezoidal method are also provided here. With regard to Runge-Kutta method such as the widely used Runge-Kutta-Fehlberg algorithm (called RKF45), the triangular factorization and the network equation are needed to be solved six times to calculate the right hand function value of RKF45, and therefore the computational cost of RKF45 to solve DAEs for one single step could be approximated by

$$C_{RK45}=6(C_1+C_2) \tag{33}$$

For the Newton-Raphson technique embedded implicit trapezoidal method, as the Jacobi matrix of Newton-Raphson is changed at each iteration, the triangular factorization matrix is needed to be updated accordingly. Therefore, if Newton-Raphson technique needs $N_{iter}$ iterations to solve the discretized nonlinear equations resulted from the implicit integration, the computational cost of the trapezoidal method for solving DAEs in one step would be

$$C_{Tra}=N_{iter}\times(C_1+C_2) \tag{34}$$

Compared $C_1$, $C_2$ and $C_3$ in (28)-(30), $C_1$ is a cubic term of generator number $N_g$ and thus is the determinant part of computational cost for one integration step. Generally speaking, the Newton-Raphson technique needs several to dozens of iterations to converge, and therefore the Newton-Raphson embedded trapezoidal method is with similar or more calculation burden than Runge-Kutta method for one single step based on the comparisons of (33) and (34), however, the former possibly has a larger integration step for time domain simulation as trapezoidal method is an implicit integration algorithm.

***E) Remarks for the proposed approach***

With regard to Fig.1, we would give the following remarks to highlight the salient features of proposed approach.

1) In order to establish a spatially paralleled transient stability analysis approach, as the state variables of differential equation $F(\mathbf{X},\mathbf{Z},t)$ in (1) are essentially independent of each other, only the power network equation $G(\mathbf{X},\mathbf{Z},t)$ needs to be decoupled and solved in parallel. For the proposed spatially paralleled hybrid approach in Fig.1, the procedures of deriving the high-order derivatives of state variables (highlighted in blue dashed boxes) are self-explained in parallel as the calculation procedure of $i^{\text{th}}$ generator only depends on the variables with index $i$ in (13)(14) and (19)-(24), while the power network equations are rearranged by the elaborated BBDF to decompose the high-order derivatives of generator terminal voltage by (26) and (27) in parallel (highlighted in red dashed boxes). This observation accommodates the proposed spatially paralleled hybrid approach with the flexibility and scalability to other complex dynamic components for transient stability analysis. For example, when more dynamic models such as the HVDC or FACTS are included in the transient stability simulation, the state variables of these dynamic models could be also solved by integration methods based on its own dynamic blocks, and the high-order derivatives of generator terminal voltage are still only coupled by the power network equation (18) and could be solved in parallel by (26) and (27) as normal. Therefore the proposed hybrid approach is suitable for transient stability analysis of power system with any complex dynamic models. Furthermore, based on (26) and (27), the partitioned subsystems and coordinated-bus cluster exchanged very limited equivalent key boundary data for carrying out the transient stability simulation, and therefore the proposed approach is absolutely with a good data privacy, which is very practical and significant for a regional system operator who might be not possible to obtain all the data, e.g., operational or parameter data of other regions.

2) It is noted that in (11), the admittance matrix $\left(\hat{\mathbf{Y}}_n+\hat{\mathbf{Y}}_g(\delta)\right)$ is a dynamic matrix related to the generator angle δ. When using the first order derivative based algorithm to conduct the integration for the differential equation $F(\mathbf{X},\mathbf{Z},t)$, the maximal stable integration step is very small due to the limited mathematical stability region according to (15), and thus the admittance matrix $\left(\hat{\mathbf{Y}}_n+\hat{\mathbf{Y}}_g(\delta)\right)$ needs to be updated frequently at each small integration step. When utilizing the triangular factorization strategy for decomposing the admittance matrix $\left(\hat{\mathbf{Y}}_n+\hat{\mathbf{Y}}_g(\delta)\right)$, the triangular factorization reuse efficiency is not high. However, as the proposed hybrid approach takes advantages of high-order derivatives of state variables, it has a large mathematical stability region resulting in a large integration step for solving differential equations according to (15). As a result, the admittance matrix $\left(\hat{\mathbf{Y}}_n+\hat{\mathbf{Y}}_g(\delta)\right)$ of proposed approach is updated not so frequently. According to (31), regardless of how high the derivative order of state variables is, the dynamic admittance $\left(\hat{\mathbf{Y}}_n+\hat{\mathbf{Y}}_g(\delta)\right)$ is unchanged for calculating the high-order derivatives $\hat{\mathbf{V}}_t^{(m)}$ and $\hat{\mathbf{V}}_j^{(m)}$ at the same integration step for $m$=0,1,2,…, and thus once the triangular factorization for $\left(\hat{\mathbf{Y}}_n+\hat{\mathbf{Y}}_g(\delta)\right)$ is completed for computing first-order derivatives of generator terminal voltage, this factorization matrix could be reused for calculating the high-order derivatives of generator voltages by (26) and (27) without any extra effort for the proposed approach, and thus the triangular factorization recursive utilization rate of the proposed hybrid approach is significantly boosted.

3) Further investigating the iterative procedures in (26) and (27), the proposed hybrid approach involves iterations for passing the equivalent high-order derivatives of network boundary variables between the coordinated cluster and subsystems, and may aggravate the computation burden and communication traffic from the aspect of a single integration step. However, as the proposed approach based on the high-order derivatives could adopt a large integration step according to (15), the proposed approach will complete the whole transient stability simulation with very few numbers of numerical integration. In a whole, the efficiency promotion due to few numerical integration steps outweighs the efficiency deterioration of passing very limited key data among boundaries, therefore the proposed hybrid distributed approach finally is very efficient for power system transient stability analysis as demonstrated by the case studies in Section IV.

## IV. CASE STUDY

With the development of electronic chips and enhanced performance of personal computers (PCs), it is easy to set up a cost effective distributed computing platform using multiple PCs. Therefore in this paper, a parallel computation platform is conveniently deployed based on several identical PCs using MATLAB Distributed Computing Server and Parallel Computing Toolbox. With the tested power network partitioned into multiple subsystems and one coordinated area, each PC is either responsible to calculate the state variables of a subsystem and send the corresponding boundary variables to the coordinated area, or responsible to coordinate and send back the splitting variables to multiple subsystems. In the following three case studies, four typical integration algorithms are adopted to conduct the transient stability: 1) the first is the so-called parallel Euler method based on Euler algorithm implemented with BBDF strategy; 2) the RKF45 (ode45 in MATLAB) is a preferential solver used in MATLAB Simulink capable of conducting power system dynamic simulations with power electronic devices. RKF45 is a method of order $O(h^4)$ with an error estimator of order $O(h^5)$. By performing one extra calculation, the integration error can be effectively controlled while the integration step is automatically determined. In the following case studies, the ode45 solver in MATLAB with a self-adaptive step size will be used as the second integration algorithms for transient stability analysis; 3) As implicit trapezoidal method (named ode23t in MATLAB) is a widely used ODE solver with the excellent numerical stability, the ode23t solver is embedded with BBDF resulting in the hybrid trapezoidal method in [18] to make comparisons with the proposed approach; 4) the last is the proposed spatially paralleled hybrid approach.

### *A) Case 1: New England 10-generator 39-bus system*

The New England 10-generator 39-bus system [31] is used as the first benchmark to test the proposed approach, and this system is decomposed into four parts: three subsystems and one coordinated-bus cluster including the bus 1, 4, 14 and 17 as shown in Fig. 2. The condition for transient stability analysis is settled as follows: 1) a three-phase ground fault occurs at transmission line 16-24 near bus 16 and is removed after 0.18s by cutting off the line; 2) the total simulation time is 3s and the generator damping ratio is assumed to be 0.05; 3) to achieve the preset accuracy that the angle differences from the authentic results should be no more than 3 degrees during the whole transient simulation period, the integration step of proposed approach is 0.06s for the derivative order $m_{end}$=8, and the Euler algorithm is configured with a integration step 0.005s, while the integration step of RKF45 and trapezoidal method is automatically determined by ode45 and ode23t according the preset accuracy.

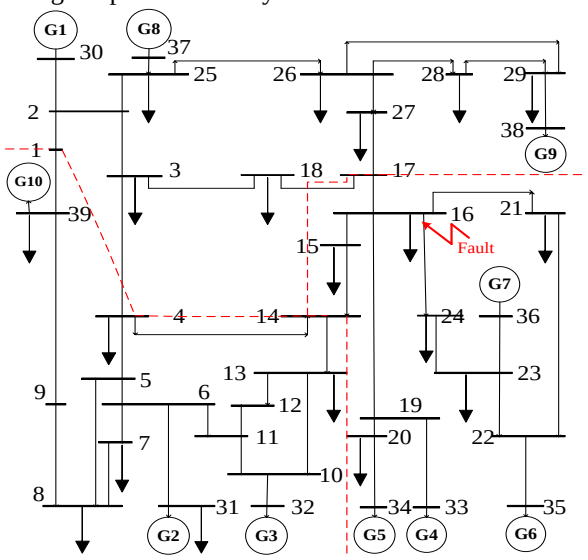

Fig. 2 Partitions of New England 10-generator 39-bus system

Fig.3(a)-(d) demonstrates the generator angles solved by the parallel Euler method, the RKF45, the Trapezoidal and the proposed spatially paralleled hybrid approach with the maximum swing amplitude of the $5^{th}$ generator highlighted in thick line. Furthermore, the authentic results and the maximum errors for the four methods among all buses are indicated by the $5^{th}$ generator angles in Fig.3 (e). As demonstrated by these figures, the generator angles of four methods match well with each other during the time domain simulation period. To further compare the solution quality of these algorithms, Table 1 shows the magnitudes of the $5^{th}$ generator angle during the whole 3s simulation period with an interval of 0.12s. As shown in Table 1, the solutions of all the methods are very similar and the maximal errors of any two algorithms are within 3 degrees which well satisfy the accuracy requirement. In the view point of time consuming, the parallel Euler, the RKF45, the Trapezoidal and the proposed hybrid approach spends 0.296s, 0.235s, 0.224s and 0.134s to finish the transient stability simulation, respectively. The enhanced ratio of proposed approach compared with other three methods is 0.296s/0.134s=2.21, 0.235s/0.135=1.74, 0.224s/0.135s=1.66. The computational efficiency of proposed approach is almost doubled that of other three methods, and thus the proposed approach is the most efficient method for New England system transient stability analysis.

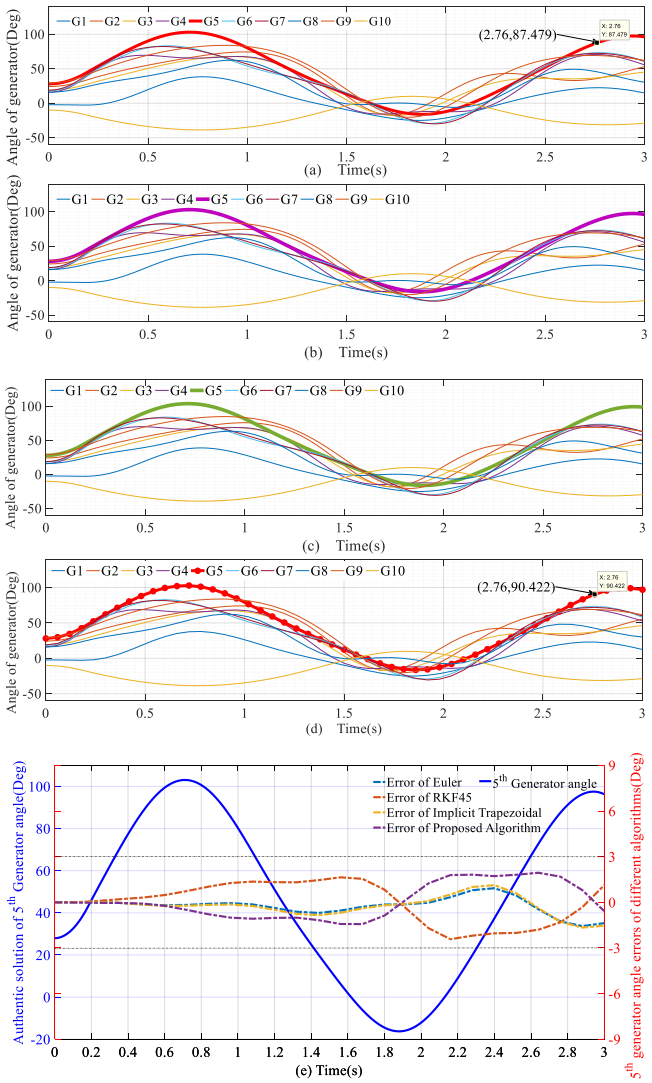


(a) Euler; (b) RKF45; (c) implicit Trapezoidal; (d) proposed approach; (e) 5th generator authentic angles and errors of different algorithms

Fig. 3 Generator angle comparisons in New England system

Table 1 Comparisons of 5*th* generator angles

| Time step (s) | Generator angles (Deg.) | | | |
|---|---|---|---|---|
| | Euler | RKF45 | Trapezoidal | Proposed |
| 0.00 | 27.971 | 27.971 | 27.971 | 27.971 |
| 0.12 | 34.517 | 34.517 | 34.538 | 34.504 |
| 0.24 | 52.465 | 52.549 | 52.481 | 52.422 |
| 0.36 | 71.396 | 71.650 | 71.399 | 71.399 |
| 0.48 | 88.009 | 88.459 | 87.996 | 88.067 |
| 0.60 | 99.396 | 100.068 | 99.362 | 99.357 |
| 0.72 | 103.037 | 103.943 | 102.984 | 102.714 |
| 0.84 | 98.056 | 99.184 | 97.984 | 97.369 |
| 0.96 | 85.594 | 86.917 | 85.503 | 84.641 |
| 1.08 | 68.711 | 70.211 | 68.604 | 67.771 |
| 1.20 | 51.069 | 52.765 | 50.944 | 50.414 |
| 1.32 | 34.872 | 36.806 | 34.732 | 34.483 |
| 1.44 | 20.164 | 22.317 | 20.016 | 19.691 |
| 1.56 | 6.272 | 8.459 | 6.132 | 5.391 |
| 1.68 | -6.140 | -4.304 | -6.248 | -7.280 |
| 1.80 | -14.481 | -13.500 | -14.530 | -15.208 |
| 1.92 | -15.777 | -16.069 | -15.749 | -15.459 |
| 2.04 | -9.074 | -10.743 | -8.963 | -7.803 |
| 2.16 | 3.807 | 1.048 | 3.984 | 5.261 |
| 2.28 | 19.944 | 16.955 | 20.156 | 20.965 |
| 2.40 | 37.373 | 34.407 | 37.575 | 38.167 |
| 2.52 | 55.295 | 52.839 | 55.444 | 56.661 |
| 2.64 | 72.743 | 71.398 | 72.811 | 75.142 |
| 2.76 | 87.479 | 87.468 | 87.460 | 90.422 |
| 2.88 | 96.303 | 97.543 | 96.205 | 98.667 |
| 3.00 | 96.298 | 98.795 | 96.132 | 97.083 |
| Time cost(s) | 0.296 | 0.235 | 0.224 | 0.134s |

To further investigate the relationship between the derivative orders, the integration step and the computational time, the relevant data are provided in the first three rows of Table 2. As shown in Table 2, with the growing derivative order, the integration step of proposed approach could always be increased accordingly to achieve the required accuracy (differences should be no more than 3 degrees with regard to authentic results). However, the increasing derivative order with enlarged integration step does not result in the monotonically decreased time cost. Fig.4 a) plots the computational cost for step-by-step changed derivative orders, and the tradeoff in term of the minimal numbers of multiplication calculation is obtained at the derivative order $m_{end}$=8 and integration step as 0.06s. This trade-off point well matches with the least time consuming 0.134s in Table 2, which indicates that (32) is an effective strategy for searching the optimal derivative order. This is because that with the growing derivative order, the calculation effort nonlinearly increases to compute the high-order derivatives, while the bearable integration step is raised slowly for the order $m_{end}$>8. As a result, a compromised point exists with the minimal time consuming 0.134s for the optimal derivative order as 8 for transient stability simulation.

Table 2 Invaginations of integration step and time cost

| Derivatives Order | | 2 | 4 | 6 | **8** | 10 | 12 | 14 |
|---|---|---|---|---|---|---|---|---|
| New England system | Integration step (s) | 0.015 | 0.03 | 0.045 | **0.06** | 0.07 | 0.075 | 0.08 |
| | Time cost (s) | 0.243 | 0.201 | 0.165 | **0.134** | 0.156 | 0.198 | 0.214 |
| IEEE 50 generator system | Integration step (s) | 0.015 | 0.035 | 0.055 | 0.07 | 0.085 | **0.1** | 0.11 |
| | Time cost (s) | 1.862 | 1.495 | 1.204 | 1.042 | 0.896 | **0.783** | 0.877 |

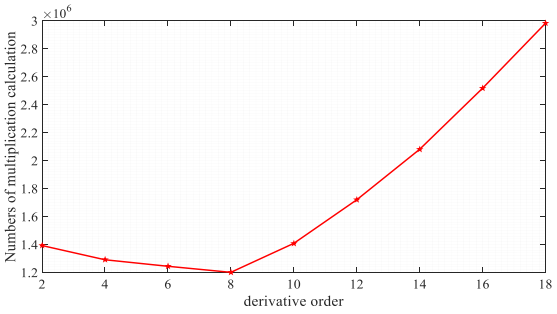


(a) New England 10-generator 39-bus system

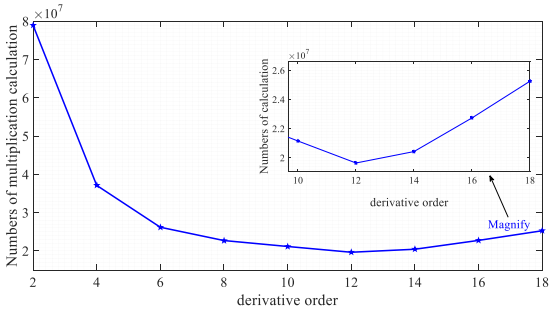


(b) IEEE 50-generator 145-bus system

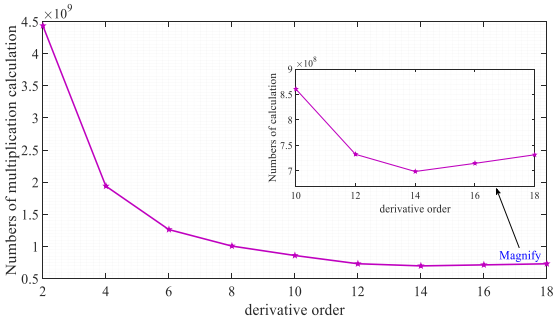


(c) Extended 200-generator 580-bus system

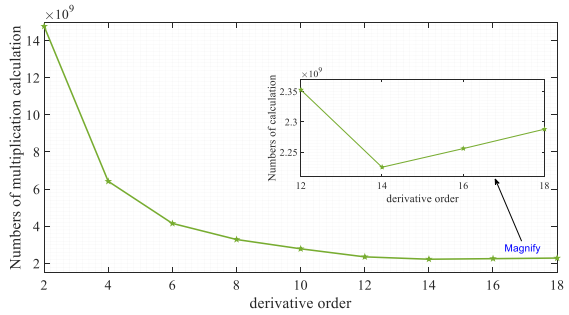


(d) Extended 300-generator 870-bus system

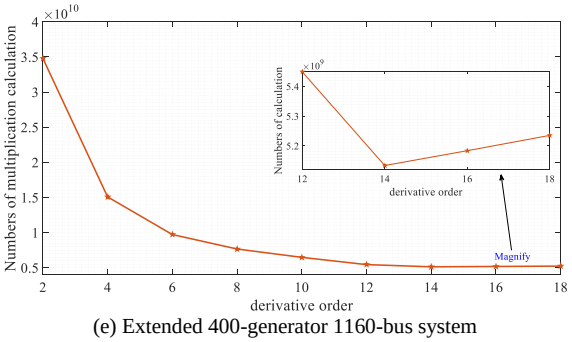


(e) Extended 400-generator 1160-bus system

Fig. 4 Trade-off for computational cost and derivative order

*B) Case 2: IEEE 50-generator 145-bus system*

The IEEE 50-generator 145-bus system [32] is selected as the second benchmark to test the proposed approach, and this large system is partitioned into four roughly equal subsystems and one coordinated-bus cluster by METIS [30]. A three-phase ground fault is assumed to occur at transmission line 57-56 near bus 57 and cleared after 0.2s by removing this line. The transient simulation period is 3s. The aforementioned four integration methods are also tested by this case study. To maintain the aforementioned accuracy (differences no more than 3 degrees), the integration step of Euler method is configured as 0.005s, and the integration step of proposed approach is optimized as 0.1s for the derivative order $m_{\text{end}}$=12, while the integration step of RKF45 and trapezoidal method is automatically controlled by ode45 and ode23 according the preset accuracy.

The angles of 50 generators during transient simulation solved by implicit trapezoidal method and the proposed parallel hybrid approach are shown in Fig.5 (a) and (b), with the maximum angle swing amplitude of the 6$^{th}$ generator highlighted in thick line. The authentic results and the maximum errors of the four methods are plotted in Fig.3 (e), which clearly demonstrated that the generator angles of these four algorithms are coherent to each other. To further investigate the generator angle differences in detail, Table 3 provides the 6$^{th}$ generator angular solutions (indicated as bold line in Fig.5 (a) and (b)) solved by the four integration methods with an interval of 0.1s. The results demonstrate that the maximum angular differences occur at 2.3s with an absolute value 2.1 degrees, which well satisfies the accuracy requirement. With regard to the consuming time, the parallel Euler, the RKF45, the Trapezoidal and the proposed hybrid approach spends 2.364s, 2.192s, 2.126s and 0.783s to finish the transient stability simulation, respectively. The speedup ratio of proposed approach is 2.364s/0.783s=3.01, 2.192s/0.783s=2.80, 2.126s/0.783s=2.72. From these results, the proposed hybrid approach is with the triple calculation efficiency and satisfied accuracy compared with other three integration algorithms for the transient stability analysis of IEEE 145-bus system.

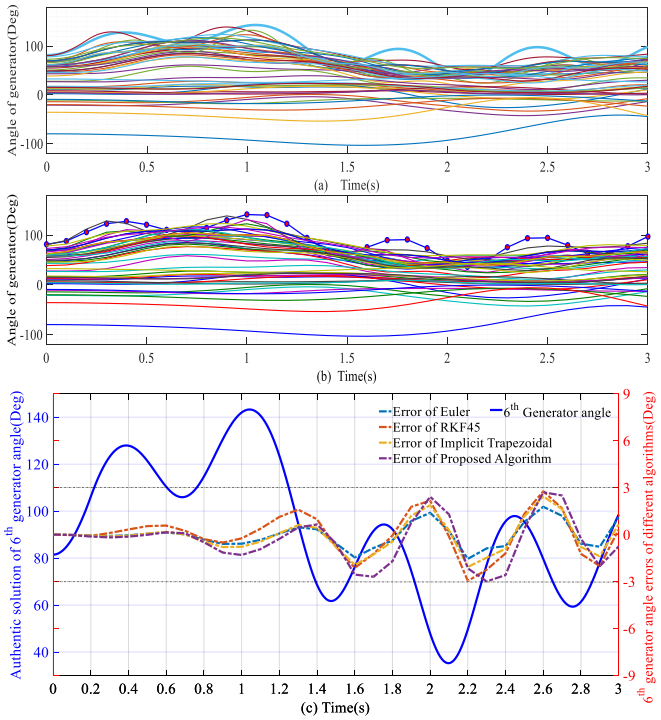


(a) implicit trapezoidal method; (b)proposed approach; (c) 6$^{th}$ generator authentic angles and errors of different algorithms

Fig. 5 Generator angle comparisons in 50-gen system

Table 3 Comparison of 6$^{th}$ generator angles of 50-gen system

| Time step (s) | Generator angles (Deg.) | | | |
|---|---|---|---|---|
| | Euler | RKF45 | Trapezoidal | Proposed |
| 0.0 | 81.474 | 81.474 | 81.474 | 81.474 |
| 0.1 | 88.155 | 88.149 | 88.150 | 88.143 |
| 0.2 | 106.217 | 106.197 | 106.197 | 106.156 |
| 0.3 | 123.185 | 123.374 | 123.150 | 123.089 |
| 0.4 | 127.875 | 128.250 | 127.850 | 127.789 |
| 0.5 | 121.332 | 121.815 | 121.339 | 121.262 |
| 0.6 | 110.326 | 110.761 | 110.360 | 110.334 |
| 0.7 | 106.091 | 106.318 | 106.082 | 106.163 |
| 0.8 | 114.857 | 114.899 | 114.737 | 114.697 |
| 0.9 | 130.782 | 130.864 | 130.579 | 130.226 |
| 1.0 | 142.174 | 142.518 | 141.978 | 141.455 |
| 1.1 | 140.741 | 141.453 | 140.627 | 140.150 |
| 1.2 | 123.534 | 124.594 | 123.554 | 123.194 |
| 1.3 | 94.501 | 95.633 | 94.644 | 94.489 |
| 1.4 | 68.500 | 69.134 | 68.591 | 68.808 |
| 1.5 | 62.662 | 62.447 | 62.459 | 62.667 |
| 1.6 | 76.668 | 75.997 | 76.195 | 75.569 |
| 1.7 | 91.988 | 91.615 | 91.578 | 90.150 |
| 1.8 | 92.309 | 92.627 | 92.241 | 90.979 |
| 1.9 | 74.047 | 74.955 | 74.388 | 73.932 |
| 2.0 | 47.417 | 48.191 | 47.900 | 48.443 |
| 2.1 | 35.217 | 34.875 | 35.281 | 36.285 |
| 2.2 | 50.167 | 48.753 | 49.647 | 49.556 |
| 2.3 | 77.805 | 76.445 | 77.209 | 75.694 |
| 2.4 | 95.804 | 95.338 | 95.628 | 93.951 |
| 2.5 | 95.030 | 95.547 | 95.388 | 94.609 |
| 2.6 | 78.966 | 79.963 | 79.631 | 79.895 |
| 2.7 | 62.152 | 62.627 | 62.577 | 63.452 |
| 2.8 | 61.606 | 60.956 | 61.395 | 61.925 |
| 2.9 | 78.804 | 77.573 | 78.191 | 77.563 |
| 3.0 | 98.980 | 98.192 | 98.535 | 97.118 |
| Time cost (s) | 2.364 | 2.192 | 2.126 | 0.783 |

Furthermore, we also investigated the connections among the derivative order, the integration step and time cost for this large-scale system. As illustrated by the data in the fourth and fifth rows of Table 2, with the increasing derivative order, the integration step of proposed approach could be elongated to achieve the required accuracy, while the minimal time

consumption is 0.783s for derivative order $m_{end}$=12 and integration step 0.1s as the trade-off point. The strategy (32) is also used to evaluate the numbers of multiplication calculation for proposed approach, and Fig. 4b) clearly indicated that the optimal derivative order as 12 is the trade-off point with the minimal numbers of calculations as $1.964*10^7$, which is consistent with the minimal time cost 0.783s in Table 2.

*C) Case 3: Expanded 200-generator 580-bus system*

To further investigate the performance of proposed approach for large-scale power system transient stability analysis, the aforementioned 50-generator 145-bus system was duplicated four times and interconnected properly by adding 18 transmission lines with appropriate impedance parameters to create a larger meshed network, which has 200 dynamic generators, 580 buses and 1830 transmission lines, respectively. The same three-phase ground fault as for IEEE 145-bus system is assumed to occur at transmission line 57-56 near bus 57 and cleared after 0.2s by cutting off this line. The integration step of implicit trapezoid method is automatically controlled by ode23t according the settled accuracy, while the optimal derivative order is $m_{end}$=14 with an integration step as 0.1s for the proposed approach, which could be determined from the minimal value of (32) and indicated the trade-off point in Fig.4 c).

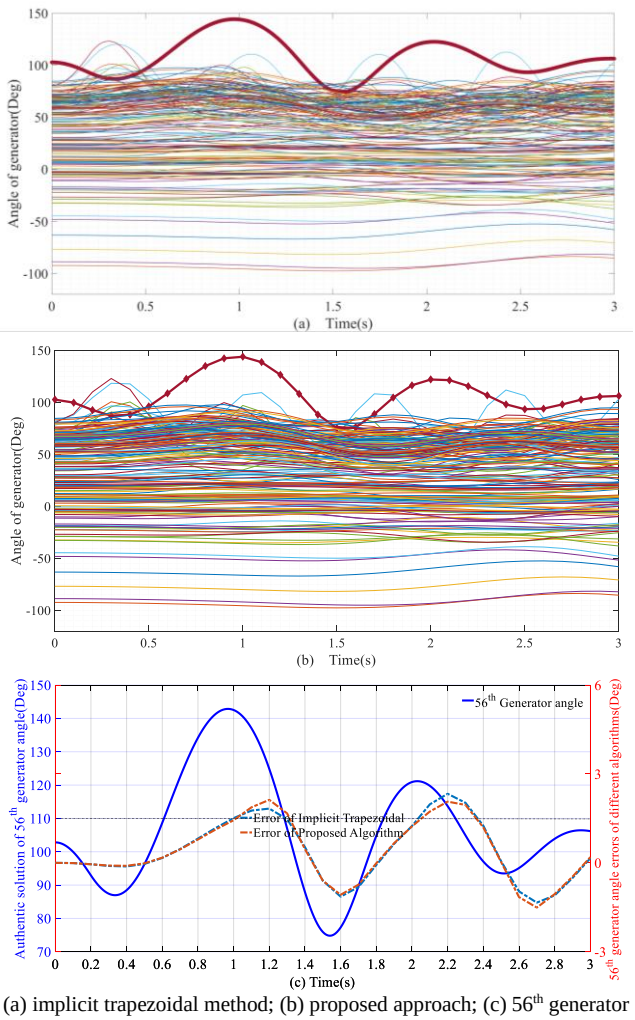


(a) implicit trapezoidal method; (b) proposed approach; (c) 56th generator authentic angles and errors of implicit trapezoidal and proposed approach

Fig. 6 Generator angle comparisons of 200-generator system

The angles of 200 generators solved by the implicit trapezoid method and the proposed parallel hybrid approach in time domain simulation are plotted in Fig.6 (a) and (b), with the maximum angle swing amplitude of the 56th generator highlighted in thick line. Fig.6 (c) further plots the authentic results and the maximum errors in term of the 56th generator angles, which clearly show that the generator angles solved by these two algorithms are very similar. With regard to the time consuming for transient stability analysis, the implicit trapezoid method and the proposed approach respectively spend 42.36s and 12.15s to solve satisfied generator angles. The time cost of implicit trapezoid method is much more expensive than the proposed approach for transient stability analysis, because the parameters $C_1$ in (34) is nonlinearly greatly increased for a large number of 200 generators and the Newton-Raphson technique also needs more iteration to converge resulting in a slightly larger $N_{iter}$ in (34) compared with that of IEEE 50-genrator system. These simulation results have demonstrated that the proposed approach is very effective and also computational efficient for transient stability analysis of large-scale power systems.

To investigate the relationship between the network scale and the optimal derivative orders, the computational burden of the extended 870-bus and 1160-bus system, which are formulated by duplicating the IEEE 50-generator 145-bus system respectively for six times and eight times with properly interconnected transmission lines, is further calculated according to (31) and (32). As shown in Fig. 4(d) and 4(e), these two systems both have a trade-off at the derivative order 14. When further make comparisons among Fig. 4(b), 4(c), 4(d) and 4(e), the IEEE 145-bus system is with an optimal derivative order as 12 while the extend 580-bus, 870-bus and 1160-bus systems are all with the optimal derivative order as 14. As these four power networks have the same time-scale generator dynamic models with control systems and their time domain simulation are set with the same accuracy requirements, the appropriate integration step $h_p$ in (32) are very similar. As a result, the optimal derivative orders of these four networks are very similar, which should be exactly determined by (32). In general, the calculation burden of one power network is closely related to the required accuracy of time domain simulation and the time-scale of dynamic models involved, and these factors will affect the optimal derivative, which does not have a necessary correlation with the network scale and should be determined from (32).

## V. Conclusion

In this paper, a spatially paralleled hybrid approach incorporating the high-order Taylor series algorithm with the block bordered diagonal form (BBDF) was proposed to improve the computational efficiency of power system transient stability analysis. The proposed approach only exchanged limit key boundary information among the partitioned power sub-networks and the coordinated-bus cluster based on BBDF, and enhanced the triangular factorization recursive utilization rate with a large integration step for transient stability simulation. It is also very flexible to accommodate any dynamic components for power system

transient stability simulation. Tests and analysis on the New England 10-generator 39-bus, IEEE 50-generator 145-bus and expanded 200-generator 580-bus power systems demonstrated the effectiveness and efficiency of the proposed approach for power system transient stability analysis. And there is also the tradeoff time consumption of the proposed approach for transient stability analysis with the increased derivative orders and integration steps.

## REFERENCES


[1] B. Wang, B. Fang, Y. Wang, H. Liu, and Y. Liu, "Power system transient stability assessment based on big data and the core vector machine," *IEEE Transactions on Smart Grid*, vol. 7, no. 5, p. 2561-2570, Sept. 2016.

[2] L. Wang, Q. Vo, M. Hsieh, S. Ke, B. Kuan, X. Lu, and A. V Prokhorov, "Transient stability analysis of Taiwan Power System's power grid connected with a high-capacity offshore wind farm," in *Proc. 2017 IEEE 3rd International Future Energy Electronics Conference and ECCE Asia (IFEEC 2017 - ECCE Asia)*, Jun. 2017, pp. 585-590.

[3] S. Lakshmiranganatha and S. S. Muknahallipatna, "Parallel in time solution of ordinary differential equation for near real-time transient stability analysis," in *Proc. 2017 Winter Simulation Conference (WSC)*, 3-6 Dec. 2017, pp. 4592-4593.

[4] A. Farraj, E. Hammad, and D. Kundur, "On the use of energy storage systems and linear feedback optimal control for transient stability," *IEEE Transactions on Industrial Informatics*, vol. 13, no. 4, p. 1575-1585, Aug. 2017.

[5] N. Hashim, N. R. Hamzah, M. F A Latip, and A. A Sallehhudin, "Transient stability analysis of the IEEE 14-bus test system using dynamic computation for power systems (DCPS)," in *Proc. 2012 Third International Conference on Intelligent Systems Modelling and Simulation*, 8-10 Feb. 2012, pp. 481-486.

[6] J. Dutiné, C. Richter, C. Jörgens, S. Schöps, and M. Clemens, "Explicit time integration techniques for electro- and magneto-quasistatic field simulations," in *Proc. 2017 International Conference on Electromagnetics in Advanced Applications (ICEAA)*, 11-15 Sept. 2017, pp. 1482-1485.

[7] W. Rahmouni and L. Benasla, "Transient stability analysis of the IEEE 39-bus power system using gear and block methods," in *Proc. 5th International Conference on Electrical Engineering*, 29-31 Oct. 2017, pp. 1-6.

[8] S. Huang, Y. Chen, C. Shen, and S. Mei, "Dynamic simulation based on Jacobian-free Newton-GMRES methods with adaptive preconditioner for power systems," *Science China*, vol. 56, no. 08, p. 2037-2045, Aug. 2013.

[9] M. H. Haque and A. H. M. A. Rahim, "An efficient method of identifying coherent generators using Taylor series expansion," *IEEE Transactions on Power Systems*, vol. 3, no. 3, p. 1112-1118, Aug. 1988.

[10] X. F. Bai and Z. Z. Guo, "The dynamic control of order selection in fast transient stability simulation by higher order Taylor series expansions," *Automation of Electric Power Systems*, vol. 23, no. 22, p. 5-7, Nov. 1999.

[11] S. Xia, X. F. Bai, S. Chen, and Z. Z. Guo, "Transient stability calculation by multi-machine equivalent Taylor series method," *Automation of Electric Power Systems*, vol. 10, no. 34, p. 24-28, May 2010.

[12] V. Jalili-Marandi, Z. Zhou, and V. Dinavahi, "Large-Scale Transient Stability Simulation of Electrical Power Systems on Parallel GPUs," *IEEE Transactions on Parallel and Distributed Systems*, vol. 23, no. 7, p. 1255-1266, Jul. 2012.

[13] V. Jalili-Marandi and V. Dinavahi, "SIMD-based large-scale transient stability simulation on the graphics processing unit," *IEEE Transactions on Power Systems*, vol. 25, no. 3, p. 1589-1599, Aug. 2010.

[14] I. C. Decker, D. M. Falcao, and E. Kaszkurewicz, "Conjugate gradient methods for power system dynamic simulation on parallel computers," *IEEE Transactions on Power Systems*, vol. 11, no. 3, p. 1218-1227, Aug. 1996.

[15] J. A. Hollman and J. R. Marti, "Real time network simulation with PC-cluster," *IEEE Transactions on Power Systems*, vol. 18, no. 2, p. 563-569, May 2003.

[16] J. Shu, W. Xue, and W. Zheng, "A parallel transient stability simulation for power systems," *IEEE Transactions on Power Systems*, vol. 20, no. 4, p. 1709-1717, Nov. 2005.

[17] T. Tsuji, F. Magoulès, K. Uchida, and T. Oyama, "A partitioning technique for a waveform relaxation method using eigenvectors in the transient stability analysis of power systems," *IEEE Transactions on Power Systems*, vol. 30, no. 6, p. 2867-2879, Nov. 2015.

[18] S. Fan, H. Ding, K. Anuradha, and M. G. Aniruddha, "Parallel electromagnetic transients simulation with shared memory architecture computers," IEEE Transactions on Power Delivery, vol. 33, no. 1, p. 239-247, Feb. 2018.

[19] X. Liu and W. Fu, "Stabilized bordered block diagonal form for solving nonlinear magnetic field problems," IEEE Transactions on Magnetics, vol. 54, no. 3, p. 1-5, Mar. 2018.

[20] G. Aloisio, M. A. Bochicchio, M. La Scala, and R. Sbrizzai, "A distributed computing approach for real-time transient stability analysis," *IEEE Transactions on Power Systems*, vol. 12, no. 2, p. 981-987, May 1997.

[21] C. Hong, "Parallel-in-time algorithm for analysis of power system Transient stability," *Power System Technology*, vol. 4, no. 27, p. 31-35, Apr. 2003.

[22] F. Wang and Y. He, "Parallel computation of transient stability based on multi-level high-order symplectic Runge-Kutta method," *Power System Protection and Control*, vol. 11, no. 39, p. 22-32, Jun. 2011.

[23] F. Wang, "Parallel algorithm of highly parallel relaxed Newton method for real-time simulation of transient stability," *Proceedings of the CSEE*, vol. 11, no. 19, p. 14-17, May 1997.

[24] Y. Chen, C. Shen, and J. Wang, "Distributed transient stability simulation of power systems based on a Jacobian-free Newton-GMRES method," *IEEE Transactions on Power Systems*, vol. 24, no. 1, p. 146-156, Feb. 2009.

[25] P. W. Sauer and M. A. Pai, *Power system dynamics and stability*. Englewood Cliffs, NJ: Prentice-Hall, 1998.

[26] X. Wang, S. G. Ziavras, C. Nwankpa, J. Johnson, and P. Nagvajara, "Parallel solution of Newton's power flow equations on configurable chips," *International Journal of Electrical Power & Energy Systems*, vol. 29, no. 5, p. 422-431, 2007.

[27] K. W. Chan, "Parallel algorithms for direct solution of large sparse power system matrix equations," *IEE Proceedings - Generation, Transmission and Distribution*, vol. 148, no. 6, p. 615-622, Nov. 2001.

[28] P. Yamian, Y. Aimin, C. Jincai, G. Dianxuan, and Z. Shiqiu, "Numerical algorithm research for nonlinear ODEs and stability analysis in computer," in *Proc. 2009 International Conference on Test and Measurement*, 5-6 Dec. 2009, pp. 168-171.

[29] N. J. Higham, *Accuracy and stability of numerical algorithms*. Philadelphia: SIAM: Society for Industrial and Applied Mathematics, 1996.

[30] G. Karypis and V. Kumar, "Metis: a software package for partitioning unstructured graphs," *International Cryogenics Monograph*, 121-124, 1998.

[31] K. R. Padiyar, *Power system dynamics: stability and control*. Singapore: John Wiley & Sons (Asia) Pte Ltd, 1996.

[32] A. A. Fouad and V. Vittal, *Power system transient stability analysis using the transient energy function method*.

Englewood Cliffs, NJ: Prentice-Hall, 1992.

## APPENDIX

When the generator is equipped with the IEEE type I excitation system as shown in Fig.A1 for regulating its potential voltage, we have the formula (A1) for its dynamics.

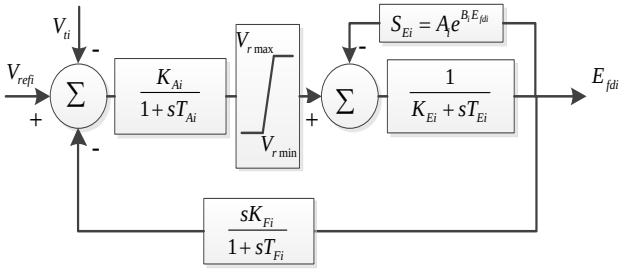


Fig.A1 Block function of IEEE type I excitation system

$$X_i^{(1)}=T_{mi}^{-1}A_{mi}\begin{bmatrix}I_{qi}\\I_{di}\\X_i\end{bmatrix}+v_i(i=1,2,...n) \tag{A1}$$

where $X_i=(E_{qi}^{'},E_{di}^{'},R_{fi},E_{fdi},V_{ri})^T$, $T_{mi}=diag(T_{di}^{'},T_{qi}^{'},T_{Fi},T_{Ei},T_{Ai})$

$$A_{mi}=\begin{bmatrix}0 & X_{di}^{'}-X_{di} & -1 & 0 & 0 & 1 & 0\\ X_{qi}-X_{qi}^{'} & 0 & 0 & -1 & 0 & 0 & 0\\ 0 & 0 & 0 & 0 & -1 & K_{Fi}/T_{Fi} & 0\\ 0 & 0 & 0 & 0 & 0 & -K_{Ei} & 1\\ 0 & 0 & 0 & 0 & K_{Ai} & -K_{Ai}K_{Fi}\big/T_{Fi} & -1\end{bmatrix} \tag{A2}$$

and $v_i=K_{Ai}(V_{refi}-V_{ti})-S_{Ei}E_{fdi}$. It is noted that $T_{mi}$ and $A_{mi}$ are constant, and therefore the high-order derivatives of $X_i$ is

$$X_i^{(m)}=T_{mi}^{-1}A_{mi}\begin{bmatrix}I_{qi}\\I_{di}\\X_i\end{bmatrix}^{(m-1)}+v_i^{(m-1)}(i=1,2,...n) \tag{A3}$$

where $\begin{pmatrix}I_{qi}\\I_{di}\end{pmatrix}^{(m-1)}=\left[T(\delta_i)\begin{pmatrix}I_{xi}\\I_{yi}\end{pmatrix}\right]^{(m-1)}=\sum_{k=0}^{m-1}C_{m-1}^{k}T^{(m-k-1)}(\delta_i)\begin{pmatrix}I_{xi}\\I_{yi}\end{pmatrix}^{(k)}$ can

be calculated based on (24) and the axis transfer matrix, and

$$v_i^{(m-1)}=(S_{Ei}E_{fdi})^{(m-1)}+[K_{Ai}(V_{refi}-V_{ti})]^{(m-1)}=\sum_{k=0}^{m-1}C_{m-1}^{k}S_{Ei}^{(k)}E_{fdi}^{(m-1-k)}-K_{Ai}V_{ti}^{(m-1)} \tag{A4}$$

1) Based on $S_{Ei}=A_ie^{B_iE_{fdi}}$, then $S_{Ei}^{(1)}=A_iB_iE_{fdi}^{(1)}e^{B_iE_{fdi}}=B_iE_{fdi}^{(1)}S_{Ei}$ and $S_{Ei}^{(k)}=B_i\sum_{j=0}^{k-1}C_{k-1}^{j}S_{Ei}^{(j)}E_{fdi}^{(k-j)}$ ($k$=2,…,$m$-1);

2) Based on $V_{ti}^2=V_{xi}^2+V_{yi}^2$, then $V_{ti}V_{ti}^{(1)}=V_{xi}V_{xi}^{(1)}+V_{yi}V_{yi}^{(1)}$ and successively differentiate its two sides by $m$-2 times, we have

$$\sum_{l=0}^{m-2}C_{m-2}^{l}V_{ti}^{(m-2-l)}V_{ti}^{(l+1)}=\sum_{l=0}^{m-2}C_{m-2}^{l}V_{xi}^{(m-2-l)}V_{xi}^{(l+1)}+\sum_{l=0}^{m-2}C_{m-2}^{l}V_{yi}^{(m-2-l)}V_{yi}^{(l+1)}$$

and the $m$-1 order derivatives of $V_{ti}$ could be calculated as (A5)

$$V_{ti}^{(m-1)}=\frac{1}{V_{ti}}[\sum_{l=0}^{m-2}C_{m-2}^{l}V_{xi}^{(m-2-l)}V_{xi}^{(l+1)}+\sum_{l=0}^{m-2}C_{m-2}^{l}V_{yi}^{(m-2-l)}V_{yi}^{(l+1)}-\sum_{l=0}^{m-3}C_{m-2}^{l}V_{ti}^{(m-2-l)}V_{ti}^{(l+1)}] \tag{A5}$$